Vaccine 29 (2011) 9423–9430

Contents lists available at SciVerse ScienceDirect

Vaccine

journal homepage: www.elsevier.com/locate/vaccine

A molecular dynamics study of loop fluctuation in human papillomavirus type 16 virus-like particles: A possible indicator of immunogenicity

Harshad Joshi [a], Srinath Cheluvaraja [a], Endre Somogyi [a], Darron R. Brown [b], Peter Ortoleva [a,*]

[a] Chemistry Department, Indiana University, Bloomington, USA
[b] Departments of Medicine, Microbiology and Immunology, Indiana University School of Medicine, Indianapolis, USA

ARTICLE INFO

Article history:
Received 26 April 2011
Received in revised form 15 August 2011
Accepted 17 October 2011
Available online 24 October 2011

Keywords:
Epitope
FG loop
Immunogenicity
Human papillomavirus
Molecular dynamics
VLP
Vaccine
Computer-aided vaccine design

ABSTRACT

Immunogenicity varies between the human papillomavirus (HPV) L1 monomer assemblies of various sizes (e.g., monomers, pentamers or whole capsids). The hypothesis that this can be attributed to the intensity of fluctuations of important loops containing neutralizing epitopes for the various assemblies is proposed for HPV L1 assemblies. Molecular dynamics simulations were utilized to begin testing this hypothesis. Fluctuations of loops that contain critical neutralizing epitopes (especially FG loop) were quantified via root-mean-square fluctuation and features in the frequency spectrum of dynamic changes in loop conformation. If this fluctuation-immunogenicity hypothesis is a universal aspect of immunogenicity (i.e., immune system recognition of an epitope within a loop is more reliable when it is presented via a more stable delivery structure), then fluctuation measures can serve as one predictor of immunogenicity as part of a computer-aided vaccine design strategy.

1. Introduction

Vaccines for prevention of cervical cancer by human papillomavirus (HPV) infection have been developed from the L1 major capsid protein [1]. The active ingredient in these vaccines (e.g., Gardasil™) is a L1 protein virus-like particle (VLP) [2–6]. These VLPs are devoid of genetic material, but conformationally resemble the structure of the intact virus. Gardasil™ is composed of L1 VLPs of HPV types 6, 11, 16, and 18, and is highly effective against infection and disease caused by these HPV types [7]. Type-specific antibodies are generated by the immune systems that are capable of neutralizing infectious HPV [8]. As more than 40 HPV types that cause genital tract disease have been identified, there is a need to expand the capabilities of current vaccines to target a broader spectrum of HPV types [9,10]. Considering the high-cost of developing vaccines, the objective of the present work is to develop a computer-aided approach to vaccine discovery. Since vaccine efficacy is tied to immunogenicity of VLPs, reliable molecular predictors for achieving computer-aided vaccine design are required. These immunogenicity predictors could be generalized for other pathogens.

HPV VLPs are assembled from 72 pentamers arranged in a $T=7$ icosahedral fashion [11–13]. The VLP surface has outwardly projecting loops containing epitopes that are recognized by the immune system [14]. These epitopes elicit the production of type-specific antibodies [8]. This type specificity arises from the diversity of epitope conformations within these loops even though the sequence homology between HPV L1 proteins is relatively high compared to other proteins encoded by the virus [15–17]. Neutralization assays of HPV16 VLPs with human sera have identified the following five loop regions: BC, DE, EF, FG, and HI [13,15,16,18] (Fig. 1). These loops contain epitopes that elicit documented antibody responses, and are more flexible than the rest of the L1 monomer, showing notable conformational differences across HPV types as observed in their X-ray structures. A mouse monoclonal antibody (H.16.V5) binds to an HPV 16 epitope within the FG [17,19]. Moreover, H.16.V5 binds strongly to VLPs having both FG and HI loops but weakly to mutant VLPs containing only the FG loop [18,20]. Mutagenesis experiments with deletion of certain H.16.V5-binding epitopes mainly from residues in the HI loop and some in the FG loop show that epitope-deleted VLPs are

Abbreviations: VLPs, virus-like particles; HPV, human papillomavirus; MD, molecular dynamics; fs, femtosecond; ps, picosecond; ns, nanosecond; RMSF, root mean square fluctuation; RMSD, root mean square deviation.

* Corresponding author at: Department of Chemistry, Indiana University, 800 E. Kirkwood Ave., Bloomington, IN 47405, USA. Tel.: +1 812 856 6000/855 2717; fax: +1 812 855 8300.
E-mail address: ortoleva@indiana.edu (P. Ortoleva).

0264-410X/$ – see front matter © 2011 Elsevier Ltd. All rights reserved.
doi:10.1016/j.vaccine.2011.10.039

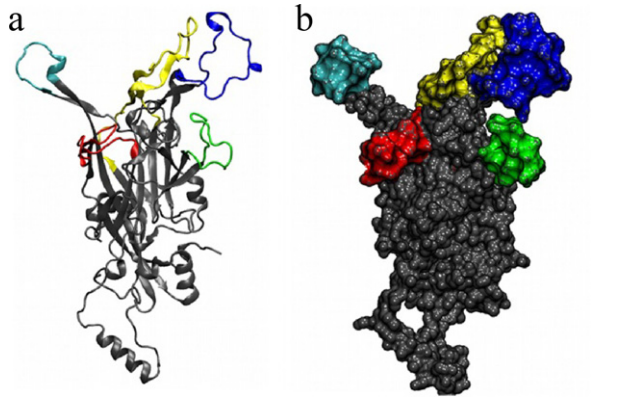

Fig. 1. L1 HPV 16-monomer in (a) cartoon and (b) surface representation with five important loop regions highlighted [12]. Color code: red – BC (residues 49–70); yellow – DE (residues 110–154); green – EF (residues 170–189); blue – FG (residues 262–291); cyan – HI (residues 347–360). (For interpretation of the references to color in this figure legend, the reader is referred to the web version of the article.)

unaffected in their reactivity to human HPV sera although their ability to bind H.16.V5 is strongly reduced [18]. However, epitope deletion reduces immunogenicity of these VLPs by a factor of at least 10–20 as compared to wild-type VLPs.

The pentameric L1 assembly is stable, and displays the epitope regions within loops described above for VLPs. Thus, L1 pentamers have been considered as vaccine candidate. An advantage of these pentameric assemblies is that they can be easily and cost-effectively produced in vitro. Pentamers are seen to be stable experimentally, but are less immunogenic than the whole VLP [21]. The relationship between immunogenicity and the structure and dynamics of epitopes incorporated in various assemblies must be clarified to facilitate the use of L1 pentamers in vaccine design.

X-ray structural studies of HPV L1 pentamers of various HPV types [11,12] show conformational differences in the loop regions containing neutralizing epitopes and provide a molecular basis for type-specificity of HPV antibodies. However, this data only provides an average of the configurations of those regions. Comparative analysis of X-ray data from HPV16 L1 pentamers and HPV16 L1 VLPs failed to discern differences in epitope conformations between these two systems [12]. However, antibody titers from mice immunized with L1 pentamers are 20–40 times lower than those produced by mice immunized with L1 VLPs [21]. ELISA shows VLP-induced antibodies are more reactive than pentamer-induced ones. Binding assays of L1 pentamers and VLPs with a variety of mouse monoclonal antibodies also show that VLPs are generally more reactive than pentamers [21].

These observations suggest that there are important structural dynamic differences between L1 pentamers and L1 VLPs not resolved with the inherently static X-ray data. Since loops FG and HI are crucial for binding to H.16.V5, the structural similarity of these epitopes in L1 pentamers and L1 VLPs suggests the possible importance of dynamic effects on immunogenicity. Therefore, a molecular dynamics (MD) study was undertaken to study behaviors of L1 assemblies of various sizes. The structural similarity of the loop regions in the pentamer and the VLP is hypothesized here to indicate that immunogenicity differences are related to fluctuation, defined here as the temporal variability in the conformation of loops containing critical epitopes. Sources of variability of loop fluctuation according to assembly size might include (1) inertial effects due to the larger versus smaller mass of the host structure; (2) the friction imposed by the host structure on the loop, and (3) atomic forces that may change according to structure, e.g., the pentamer "curvature".

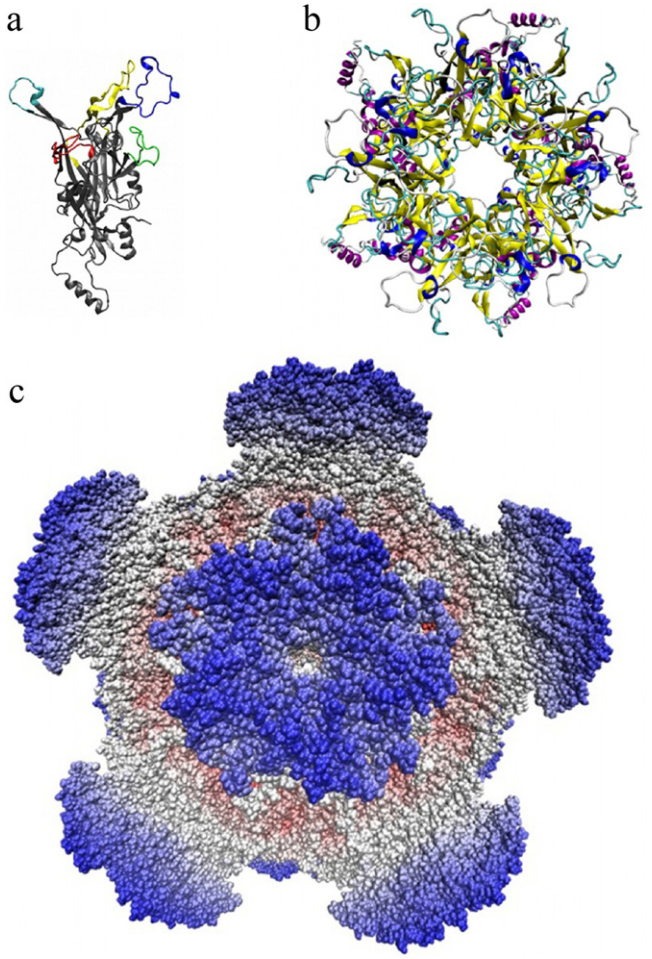

Fig. 2. Three simulated structures. (a) An isolated HPV 16 L1 monomer in cartoon representation. The protein is depicted in gray while the five important epitopes are highlighted with color code same as in Fig. 1. (b) Cartoon representation of pentameric assembly of HPV 16 L1 monomers. (c) Space filling representation of the HPV16 ($T = 1$) VLP consisting of 12 pentamers arranged in $T = 1$ icosahedral structure. (For interpretation of the references to color in this figure legend, the reader is referred to the web version of the article.)

The objective of the present study is to relate immunogenicity differences to fluctuation differences of HPV 16 loops containing critical epitopes via MD simulations by measuring quantities that distinguish atomic-level details. As MD accounts for all atomic-scale forces and dynamics, this approach accounts for the above three factors. In this way, we seek to identify quantitative measures of immunogenicity-related epitope fluctuation that can serve as an input to a Quantitative Structure–Activity Relationship (QSAR) [22] or other vaccine design approach. By comparing previously established immunogenicities of HPV L1 structures of different types, and correlating this data with differences in loop structure, a relationship between the two can be postulated and tested. Such an approach could lead to more effective, thermally stable, and cost-effective VLPs or other epitope-delivery vaccine systems.

2. Methods

2.1. Assemblies and conditions

All-atom explicit solvent MD simulations were performed on three HPV 16 L1 protein assemblies: (1) an isolated L1 monomer, (2) pentameric assembly of L1 monomers [12], and (3) the $T = 1$ VLP consisting of 12 pentamers [23] (Fig. 2). Atomic coordinates for

the monomer were obtained from the crystal structure ([23] PDB code: 1DZL; [24]), while the VLP was constructed from 60 copies of the monomer using icosahedral symmetry transformations (VIPERDB database [25]). The pentamer was extracted from this VLP construct to maintain structural continuity with the VLP. Each system was solvated with water using the solvation feature of the VMD software [26]. To match experimental conditions, the system was solvated in 0.3 M NaCl concentration using VMD autoionize feature.

2.2. Molecular dynamics simulation details

All simulations were performed with the MD software NAMD 2.7 [27] using the CHARMM27 force field [28] for proteins and the TIP3P model for water [29]. The simulated systems were kept at constant temperature using Langevin dynamics for all non-hydrogen atoms, with a Langevin damping coefficient of 5 picosecond^{-1}. A constant pressure of 1 atm was maintained using the Nosé-Hoover Langevin piston [30] with a period of 100 femtosecond (fs) and damping timescale of 50 fs.

Simulations were performed with an integration time step of 1 fs under a multiple time stepping scheme [31]; bonded interactions were computed every time step, short-range non-bonded interactions every two time steps, and long-range electrostatic interactions every four time steps. A cutoff of 12 Å was used for van der Waals and short-range electrostatic interactions; a switching function was started at 10 Å for van der Waals interactions to ensure a smooth cutoff. The simulations were performed under periodic boundary conditions, with full-system, long-range electrostatics calculated by using the particle-mesh Ewald method with a grid point density of 1/Å. The unit cell was large enough so that adjacent copies of the system did not interact via short-range interactions. Prior to simulation, each system was subjected to 1000 steps of conjugate gradient energy minimization, followed by 100 picoseconds (ps) of equilibration. We then performed all-atom molecular dynamics as described above, at 300 K for 10 ns for each system.

The $T = 1$ VLP is comprised of 428,770 atoms. Thus the largest system of $T = 1$ VLP with explicit solvent environment contains ~4 million atoms and required massive amount of parallel computing resources. The large number of atoms in the simulations is mainly due to the water included to minimize boundary effects. Minimization and equilibration were performed on 1024 cores, with performance of 750 ps/day in the case of VLP simulation.

2.3. Loop structure and fluctuation metrics

To distinguish the behavior in the simulated systems in terms of loop structures and their fluctuations, following indicators were considered.

1. *Dihedral distribution and fluctuations for individual loops*. The distribution of backbone loop dihedral angles [32] was measured. This variable indicates the conformational space explored by the loops. Similarly, fluctuations of individual atoms from their average value in a given loop type were computed. This metric indicates the conformational freedom available to the loops. The magnitude of the fluctuations is a measure of the flexibility of the loop.
2. *Power spectra*. The power spectrum provides the distribution of atomic vibration intensity across a range of frequencies. Lower frequencies represent slower motions, while high frequencies represent faster ones.

These measures were used to discriminate between the motions of a given loop type incorporated in an assembly of given size (i.e., from L1 monomer to $T = 1$ VLP).

3. Results

Simulations were designed to assess potential differences in behavior of loops between the three L1 protein assemblies and quantify them to serve as a basis of a computer-aided vaccine discovery strategy. The study focused on loops known to contain critical epitopes, some of which are neutralizing: EF, FG and HI (Fig. 1).

3.1. Dihedral distribution

Fig. 3 shows the distribution of backbone dihedral angles for EF, FG and HI loops in the three L1 assemblies. In each case, 10,000 time points were extracted from MD simulations to construct the probability distribution of loop conformations. FG followed the hypothesized assembly size trend, i.e., the dihedral angles of this loop varied over a smaller region for the VLP relative to the pentamer, and even smaller for the monomer. This trend suggested that the large flexibility of the FG loop observed in the isolated monomer diminishes when the monomer resides within larger assemblies. HI maintained more or less its native L1 conformation in the pentamer and VLP, and varied little as can be seen from Fig. 3. In contrast, EF varied over a larger region of conformational space as one proceeded from monomer to pentamer to VLP.

3.2. Positional variance

Next, the overall fluctuations of a particular loop from its average configuration were compared. Loop fluctuation is not easily quantified in X-ray or cryo-EM data. While a structure provides the most likely or average configuration, its fluctuation measures the importance of other configurations away from the average, but which may (according to our immunogenicity hypothesis) be functionally relevant. As in the introduction, dynamic information obtained from MD provides advantages over the inherently averaged experimental data. Thus, positional variance of the loop atoms was quantified as another measure of epitope fluctuation. Positional variance was computed by summing the deviation of individual backbone atom position and dividing by the number of backbone atoms in the loop. This measure is slightly different from the usual root mean square fluctuation (RMSF). RMSF measures fluctuation from a fixed reference structure by aligning two structures, thus eliminating translational and rotational motions. In contrast, average loop positional variance calculated here contains contributions from overall displacements of the loops and their motions relative to the rotation/translation and internal motions of the assembly. The overall motions potentially affect epitope location and orientation within loops; according to our hypothesis, these overall fluctuations also affect immunogenicity and binding properties of the monomer or larger assembly. Thus, including the effect of overall and internal assembly motions on loop fluctuations provides a more complete measure of their potential relevance to immunogenicity.

Positional variance is tabulated for each loop and assembly (Table 1), while plots of individual loop variance are shown (Fig. 4). Individual atomic fluctuations for loop atoms are only shown for EF, FG and HI, known to be central to immunogenicity. These positional variance measures of loop fluctuation were seen to be largest in the monomer, significantly smaller in the pentamer and even smaller for the VLP. To show the potential influence of simulation times used, averages were taken over 2 ns windows from whole

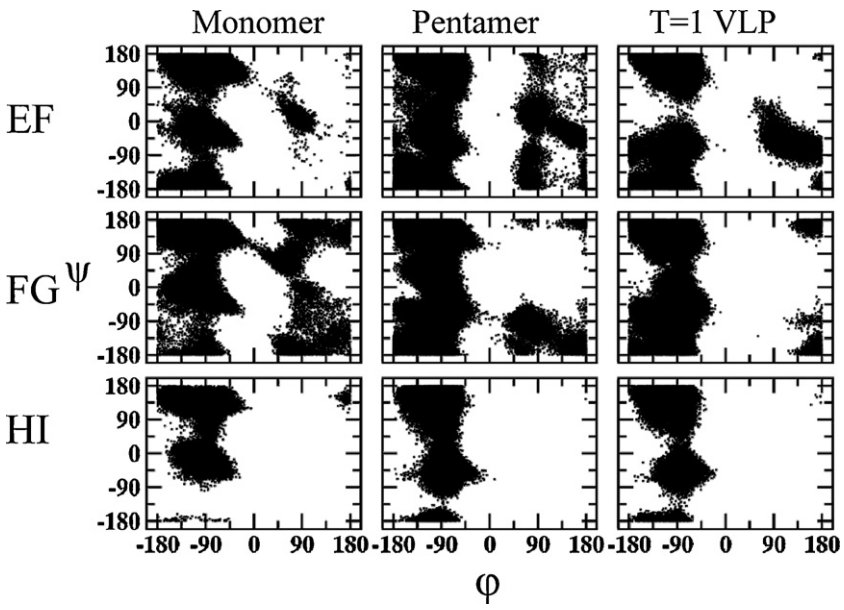

Fig. 3. Loop dihedral distribution for monomer (left), pentamer (middle) and the $T = 1$ VLP (right). Distributions are shown for EF (first row), FG (second row), and HI (third row). For each loop the x-axis (φ angle) and corresponding y-axis (ψ angle) specifies positions in the dihedral space. In general, the spread of the distributions decrease as the assembly size increases.

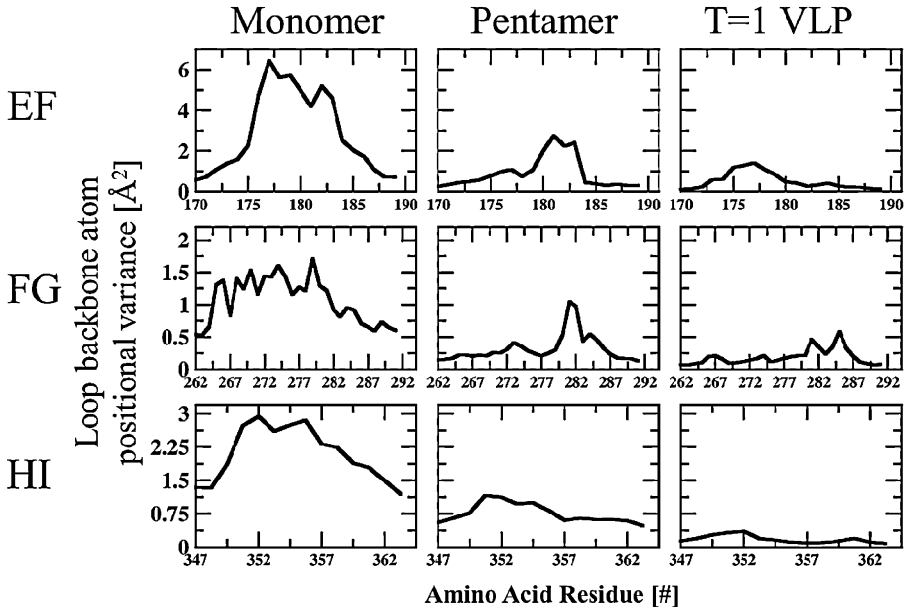

Fig. 4. Backbone atom loop positional variance for monomer (left), pentamer (middle) and the $T = 1$ VLP (right). Plots are shown for EF (first row), FG (second row), and HI loop (third row). For each loop the x-axis denotes the residue number and corresponding y-axis gives the magnitude of fluctuation in Å^2. Like the dihedral distributions (Fig. 3) the positional variance decreases as assembly size increases.

the simulation interval (10 ns) and no significant change in qualitative behavior was observed (Table 1). Fluctuations of the EF loop for the pentameric L1 structure and the L1 VLP are significantly smaller than for the monomer. Fluctuations in the monomer relative to that in the larger assemblies greatly exceeded that expected simply from the inertial effects of the larger assembly; this suggests important differences in internal fluctuations between the assemblies. The extent of motion of individual loops was then measured by RMSD from the initial structure for the L1 monomer, pentamer, and VLP at the end of simulation trajectory (10 ns) (Table 2). RMSD data in Table 2 showed that, over a 10 ns MD simulation, epitope fluctuations were largest for the monomer and smallest for the VLP.

Table 1
Positional variance (Å^2) for L1 monomer, pentamer, and VLP.

Loop	L1 monomer	Pentamer	$T = 1$ VLP
EF	8.54 ± 1.83	2.15 ± 0.81	1.89 ± 0.96
FG	6.69 ± 2.87	1.41 ± 0.64	0.85 ± 0.36
HI	10.5 ± 5.66	1.67 ± 0.48	1.12 ± 0.53

3.3. Power spectra

Power spectra from the loop conformation time series provided a third measure of fluctuation (Fig. 5). The power spectrum is a measure of the energies of the different frequency motions present in a

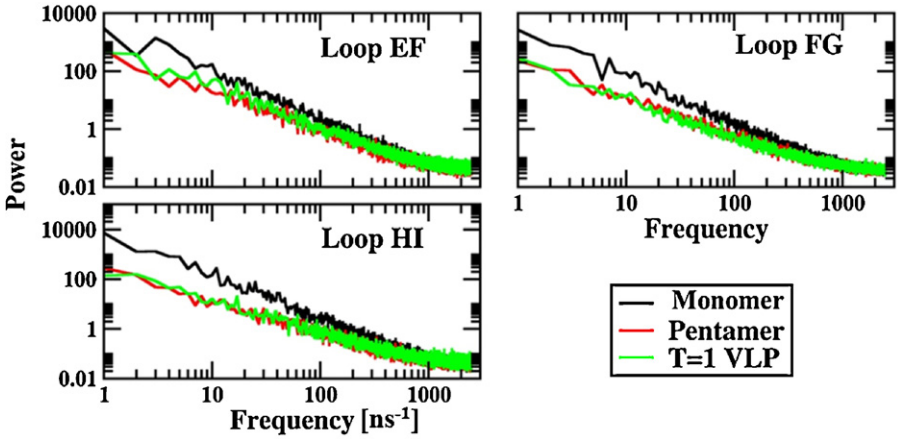

Fig. 5. Power spectrum for fluctuations in three loops: EF, FG, and HI. Frequency of the loop conformational fluctuations is indicated on *x*-axis while their averaged square magnitude is indicated on *y*-axis. Spectra for L1 monomer, pentamer and $T = 1$ VLP are indicated in black, red and green, respectively. (For interpretation of the references to color in this figure legend, the reader is referred to the web version of the article.)

Table 2
RMSD (Å) of structures in the loop regions from their initial structures at the end of 10 ns MD simulations of VLP, pentamer, and L1 monomer are shown in the first three columns. The RMSD decreases for each epitope as we move across the table.

Loop	L1 monomer	Pentamer	$T = 1$ VLP
EF	4.13	3.81	3.11
FG	4.28	2.74	2.37
HI	3.09	2.63	1.44

signal and is a commonly used to understand electrical and chemical signals. The power spectrum provides a way to identify types of motions (i.e., high versus low frequency). All loops in the monomer showed increased power in the low frequency region versus those for the pentamer and VLP (Fig. 5). At higher frequency, the power for the three cases was similar because short time-scale fluctuations are due to spatially localized processes (e.g., bond oscillations) and are similar in the three structures.

To measure relative flexibility of L1 pentamers within and outside the VLP, the RMS deviation was computed in two ways: (1) the spread of the RMS deviation from the initial structure between a monomer and a pentamer in a pentamer simulation (black and red curves, respectively, Fig. 6 upper panel), and (2) the spread of the RMS deviation from the initial structure between a monomer and a pentamer in a VLP simulation (black and red curves, respectively, Fig. 6 lower panel). Comparison of (1) and (2) showed the spread was larger in the pentamer than in the VLP, i.e., the flexibility of the pentamer is greater when it is in isolation than within the VLP.

4. Discussion

Any molecule or virus particle containing a structure recognized or bound by an immunoglobulin is known as an antigen [33]. The portion of the antigen bound to the immunoglobulin is known as the antigenic determent, or epitope. Antibody binding to epitopes may or may not result in neutralization of a virus [34]. Neutralization has been defined as "the loss of infectivity which ensues when antibody molecule binds to a virus particle, and usually occurs without any other agency" [35]. Antibody neutralization often depends on the strength of antibody binding to surface epitopes. In the case of influenza virus, this has been shown that neutralizing antibody binds primarily to the HA epitope [36]. Higher affinity of antibody binding to HA correlates directly with neutralization of influenza virus.

Burton has argued for a simple occupancy model of viral neutralization in which virus is neutralized "when a fairly large proportion of available sites on the virion are occupied by antibody, which leads to inhibition of virus attachment to host cells or interference with the entry (fusion) process" [37]. He argues that an important prediction of this model is "that the neutralizing efficacy of an antibody should be related to its affinity for antigen on the virion surface" [37]. Therefore, it is argued that the most effective vaccines should be those that elicit antibodies with high binding affinities to neutralizing epitopes, the portion of the antigen bound to the neutralizing immunoglobulin.

For HPV 16, although specific amino acid residues characterizing the neutralizing epitopes have not been completely elucidated, it is known that such epitopes exist within the FG and HI loops of L1 protein [15]. The FG and HI loops are hypervariable regions located at the tip of the capsomere that contain surface-exposed epitopes [15]. Amino acids 266 through 297 constitute the HPV 16 FG loop. The mouse monoclonal antibody H16.V5 binds to a major epitope within the FG loop, and neutralizes HPV 16 with a high degree of efficacy [15,38,39].

Ryding, et al., performed studies to characterize the epitope bound by H16.V5 monoclonal antibody [18]. They showed that mutation of L1 residues 270 and 285 led to failure of H16.V5 binding [18]. Christensen et al., transferred H16.V5 binding by transferring the HPV16 FG loop, suggesting that these two amino acid residues are included in the H16.V5 binding site [20]. The mAb H16.E70 is also neutralizing for HPV16, and appears to be directed against an epitope within FG [13]. Amino acid 282 appears to be important in the epitope bound by the H16.E70 mAb. In addition, Sadeyan, et al., showed that insertion of a six amino acid epitope of hepatitis B into the FG loop at amino acid position 266 led to lower levels of neutralizing antibody [40]. Thus, studies on VLP immunogenicity as well as antibody binding have underscored the important role played by epitopes within the FG and HI loops of L1.

Differences in FG and HI loop fluctuations between the three L1 structures (monomers, pentamers, and $T = 1$ VLPs) are likely a result of intra- and cross-monomer interactions of specific amino acid residues making up critical epitopes. In the pentamer, HI from one monomer is confined by loops EF and FG from its counterclockwise neighbor. In contrast, loop FG interacts with loops DE and HI from its clockwise neighbor. Furthermore, interaction of intra-monomer FG and HI loops is minimal because of the spatial separation between them. These spatial relationships and interactions manifest in the breadth of the dihedral variation of these loops. HI samples a narrow distribution of conformations in the VLP and the pentamer but

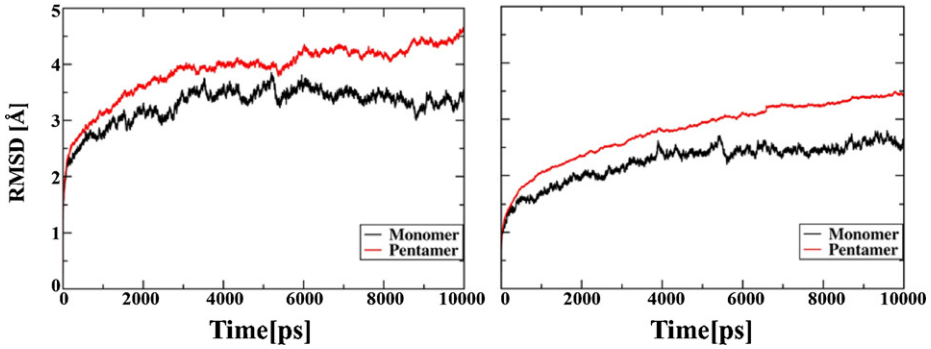

Fig. 6. (a) Comparison of RMSD of protein (black) and pentamer (red) from a pentamer simulation over a 10 ns time-course. (b) Comparison of RMSD of protein (black) and pentamer (red) from a $T = 1$ VLP simulation over a 10 ns time-course. The spread between two curves is less in (b) than in (a) indicating the reduced flexibility of pentamer within $T = 1$ VLP. (For interpretation of the references to color in this figure legend, the reader is referred to the web version of the article.)

a broad spectrum in the monomer (RMSD for HI increases 10 fold in monomer compared to pentamer and VLP), suggesting strong interactions between this loop and the neighboring monomer. HI structures obtained at the end of the pentamer and VLP simulations have small deviation from their initial one (Table 2).

FG fluctuations, on the other hand, reduce systematically in going from monomer to pentamer to VLP, and this is a result of FG–HI interactions. Table 2 shows this higher flexibility of loop FG in pentamer as compared to VLP. Antibody binding studies in ELISA assays indicate that FG is stabilized by HI by binding to antibodies when HI is present but only weakly binding in its absence. Variations in FG and HI fluctuations, in going from L1 monomeric protein to pentamer, indicate the effect of intra- or cross-monomer interactions with these loops. The change in HI fluctuation is less than that in FG, suggesting its relative lack of sensitivity to local structure. This insensitivity of HI fluctuations across the various assemblies, as predicted by the simulations, is consistent with the observed important role of HI in antibody binding in the ELISA assays.

At first the behavior of EF, with its wider dihedral distribution, seems to contradict the notion that fluctuation decreases with assembly size. Comparison of dihedral distribution of EF with that of FG, HI (Fig. 3), shows that EF exhibits different configurations in the larger assemblies than in the monomer, while FG and HI do not. EF also has negligible cross-monomer interactions, and resides in an area which is at the monomer–monomer interface for the pentamer and VLP. Therefore, it explores a different volume of configuration space in pentamer compared to monomer (Fig. 3). Going from pentamer to VLP, EF explores different regions of configuration space. This may arise from the fact that when two pentamers assemble to form VLP (Fig. 1), the close proximity of EF to regions from other pentamers prompts it to sample a different ensemble of configurations, relative to that for the isolated pentamer. Effectively, the fluctuation breadth for EF increases systematically from monomer to pentamer to VLP. This likely explains why this loop illustrates a fluctuation trend opposite to that from FG and HI. Thus, the seemingly contradictory trend can be attributed to a structural transition in the EF loop induced by the interactions between monomers in the larger assemblies. Such structural transitions are not apparent in other loops. The above results suggest the importance of loop location in mediating the dependence of fluctuation on assembly size and therefore, via the proposed hypothesis, on immunogenicity.

Interactions between loops in the monomer do not involve hydrogen bonds as the loops are well separated in space, but hydrogen bonds and direct electrostatic interactions between adjacent monomers in the pentamer and VLP have a stabilizing effect on the protein backbone and hence on the epitopes contained in the loops. In the VLP, helix h4 (posterior to HI) from one pentamer has hydrophobic interactions with helices h2 and h3 from pentamers adjacent to it at points of threefold symmetry. These interactions make the pentamer less flexible inside the VLP than when it is isolated, and thereby reducing fluctuations (Fig. 6).

The fluctuation–immunogenicity hypothesis was further probed via fluctuation power spectra. Thus, for higher immunogenicity, the loops within any L1 assembly should exhibit a power spectrum similar to that observed in the VLP (Fig. 5). Thus, the reduced immunogenicity of a pentamer relative to the VLP may be linked to differences between the red and green curves in Fig. 5.

While the $T = 7$ (~2.5 million atoms) VLP is the active constituent in the Gardasil vaccine, in this study the $T = 1$ structure (428,770 atoms) was chosen to minimize computational costs. However, the $T = 1$ assembly has pentamer-level structural similarity to the $T = 7$ assembly. Furthermore, it was a natural step in the sequence of assembly sizes, and since the proposed hypothesis is the relationship between assembly size, loop fluctuation, and immunogenicity, the authors believe it provides an adequate basis for evaluating this hypothesis. There are also immunogenicity studies using $T = 1$ structure that validate the approach [41].

5. Conclusions

The simulations presented here showed that the fluctuation change in these two loops is significantly more than in other loops as one goes from one assembly to the other, underscoring the use of the fluctuation of these loops as a potential indicator of immunogenicity. According to the proposed low-fluctuation/high-immunogenicity hypothesis, methods to minimize the fluctuations of FG and HI (similar to those observed in the VLP) could lead to higher immunogenicity of pentamer-based vaccines or those involving other scaffolds as epitope-delivery systems.

The analysis indicates important subunit interactions. For example, HI shows minimal change in fluctuations between the L1 pentamer and VLPs, whereas FG shows significant difference between the two cases. This suggests HI is mainly stabilized by intra-pentameric interactions whereas FG is stabilized to a large extent by inter-pentameric interactions. Thus differences in loop–loop and loop–monomer interactions in the various assemblies can be taken as an additional potential predictor of immunogenicity.

Results presented here have implications for QSAR and computer-aided vaccine discovery strategies. The "loop fluctuation–immunogenicity hypothesis" suggests that for similar immunogenicity in the L1 pentamer and VLP to be realized, epitopes within loops and their scaffold delivery structure must be designed to have the same level of fluctuations as for loops in the VLP. Thus, efforts to produce new vaccines with scaffolds other than pure VLPs could benefit by taking into consideration

how loop conformations and fluctuations behave in the new construct. However, caution must be taken when relating fluctuation intensity with immunogenicity as structural and dynamical features may cause apparent deviation from the hypothesized fluctuation–immunogenicity relationship. Key to unraveling this relationship is the use of MD simulations wherein the amplitude and characteristics of fluctuations is readily available for analysis. Epitopes are universal molecular aspects of immunogenicity. Therefore, even though the results obtained here were based on HPV16, it is suggested that the proposed hypothesis is a promising direction for computer-aided vaccine design strategies across a broad spctrum of pathogens.

Based on the MD results, monomer–monomer interactions reduce fluctuations by restricting the motions of the FG and HI loops. The loop fluctuation analysis shows a correlation between low fluctuation and increased assembly size which, based on prior experimental results [20], we hypothesize to imply a "low fluctuation–high immunogenicity" correlation. The studies presented here involved simulations under conditions similar to those in immunogenicity experiments. The simulations were carried out for 10 ns, a period much shorter than the characteristic time of many viral processes such as virion self-assembly. However, the main focus here is on fluctuation of loops containing critical epitopes that occur on picosecond timescale (lowest frequency of the power spectrum, Fig. 5). Therefore, a 10 ns simulation is sufficient to investigate the systematic differences in epitope fluctuations for immunogenicity studies.

Loop fluctuation appears to be one mechanism responsible for experimentally observed differences in immunogenicity between L1 pentamers and VLPs. However, other complementary measures can be used for achieving a more reliable vaccine discovery strategy and for optimizing immune response and thermal stability. These measures could be affected by external conditions such as salinity, temperature. Thus, a more comprehensive computer-aided vaccine discovery strategy could involve several distinct types of simulations. However, simulating the temporal behavior of such modified vaccine candidates may not be practical with traditional MD methods. This is because, for example, predicting the stability of a vaccine nanoparticle requires extremely long MD simulations (i.e., to predict the rate of crossing barriers to VLP disassembly). New algorithimic development is therefore necessary to enable efficienet prediction of long-time VLP behavior with all the details that a traditional MD can give. A multiscale approach that allows such simulations of large macromolecular assemblies over physiologically long timescales (hundreds of nanoseconds) has been developed [42,43]. The present work provides the starting point for the future implementation of this multifaceted approach for efficient vaccine discovery.

Acknowledgements

This project was supported in part by funds from the NSF CRC program, Indiana University METACyt project, and Indiana University Office of Vice President for Research. Computations were carried out through support of the Indiana University Information Technology Center, and the Advanced Computing Facility at Argonne National Laboratory.

Contributors: P.J.O. proposed the immunogenicity–fluctuation hypothesis; D.R.B. posed the challenge of explaining immunogenicity–assembly size relationship; H.J. and S.C. carried out MD simulations; H.J., S.C. and A.S. analyzed the MD results; H.J., S.C., D.R.B. and P.J.O. wrote the paper.

References

[1] Cervical cancer vaccines. In: Brown DR, Garland SM, DeVita VT, Lawrence TS, Rosenberg SA, editors. Cancer: principles and practice of oncology, Vol. 22, 8th ed. Lippincott Williams and Wilkins; 2008.
[2] Zhou J, Sun XY, Stenzel DJ, Frazer IH. Expression of vaccinia recombinant HPV 16 L1 and L2 ORF proteins in epithelial cells is sufficient for assembly for HPV virion-like particles. Virology 1991;185:251–7.
[3] Hagensee ME, Yaegashi N, DA G. Self-assembly of human papillomavirus type 1 capsids by expression of the L1 protein alone or by coexpression of the L1 and L2 capsid proteins. J Virol 1993;67(1):315–22.
[4] RC Rose WB, Reichman RC, Garcea RL. Expression of human papillomavirus type 11 L1 protein in insect cells: in vivo and in vitro assembly of viruslike particles. J Virol 1993;67(4):1936–44.
[5] Neeper MP, Hofmann KJ, KU J. Expression of the major capsid protein of human papillomavirus type 11 in *Saccharomyces cerevisae*. Gene 1996;180(1–2):1–6.
[6] Kirnbauer R, Taub J, Greenstone H, Roden R, Dürst M, Gissmann L, et al. Efficient self-assembly of human papillomavirus type 16 L1 and L1-L2 into virus-like particles. J Virol 1993;67:6929–36.
[7] Koutsky LA, Ault KA, Wheeler CM, Brown DR, Barr E, Alvarez FB, et al. A controlled trial of a human papillomavirus type 16 vaccine. N Engl J Med 2002;347:1645–51.
[8] Christensen ND, Kreider JW. Antibody-mediated neutralization in vivo of infectious papillomaviruses. J Virol 1990;64(7):3151–6.
[9] Smith JS, Lindsay L, Hoots B, Keys J, Franceschi S, Winer R, et al. Human papillomavirus type distribution in invasive cervical cancer and high-grade cervical lesions: a meta-analysis update. Int J Cancer 2007;121(3):621–32.
[10] zur Hausen H. Human papillomavirus & cervical cancer. Indian J Med Res 2009;130(3).
[11] Bishop B, Dasgupta J, Chen X. Structure-based engineering of papillomavirus major capsid L1: controlling particle assembly. Virol J 2007;4:p3.
[12] Bishop B, Dasgupta J, Klein M, Garcea RL, Christensen ND, Zhao R, et al. Crystal structures of four types of human papillomavirus L1 capsid proteins. J Biol Chem 2007;282(43):31803–11.
[13] Roden R, Armstrong A, Haderer P, Christensen ND, Hubbert NL, Lowy DR, et al. Characterization of a human papillomavirus type 16 variant-dependent neutralizing epitope. J Virol 1997;71(8):6247–52.
[14] Senger T, Becker MR, Schädlich L, Waterboer T, Gissmann L. Identification of B-cell epitopes on virus-like particles of cutaneous alpha-human papillomaviruses. J Virol 2009;83(24):12692–701.
[15] Carter JJ, Wipf GC, Madeleine MM, Schwartz SM, Koutsky LA, Galloway DA. Identification of human papillomavirus type 16 L1 surface loops required for neutralization by human sera. J Virol 2006;80(10):4664–72.
[16] Roth SD, Sapp M, Streeck RE, Selinka HC. Characterization of neutralizing epitopes within the major capsid protein of human papillomavirus type 33. Virol J 2006;3(83).
[17] White WI, Wilson SD, Palmer-Hill FJ, Woods RM, Ghim S, Hewitt LA, et al. Characterization of a major neutralizing epitope on human papillomavirus type 16 L1. J Virol 1999;73(6):4882–9.
[18] Ryding J, Dahlberg L, Wallen-Öhman M, Dillner J. Deletion of a major neutralizing epitope of human papillomavirus type 16 virus-like particles. J Gen Virol 2007;88:792–802.
[19] White WI, Wilson SD, Bonnez W, Rose RC, Koenig S, Suzich JA. In vitro infection and type-restricted antibody-mediated neutralization of authentic human papillomavirus type 16. J Virol 1998;72(2):959–64.
[20] Christensen ND, Cladel NM, Reed CA, Budgeon LR, Embers ME, Skulsky DM, et al. Hybrid papillomavirus L1 molecules assemble into virus-like particles that reconstitute conformational epitopes and induce neutralizing antibodies to distinct HPV types. Virology 2001;291(2):324–34.
[21] Thönes N, Herreiner A, Schädlich L, Piuko K, Müller M. A direct comparison of human papillomavirus type 16 L1 particles reveals a lower immunogenicity of capsomeres than viruslike particles with respect to the induced antibody response. J Virol 2008;82(11):5472–85.
[22] Hanch C, Leo A, Hoekman D. Exploring QSAR-hydrophobic and electronic, and steric constants. Washington, DC: American Chemical Society; 1995.
[23] Chen XS, Garcea RL, Goldberg I, Casini G, Harrison SC. Structure of small virus-like particles assembled from the L1 protein of human papillomavirus 16. Mol Cell 2000;5(3):557–67.
[24] Berman HM, Westbrook J, Feng Z, Gilliland G, Bhat TN, Weissig H, et al. The protein data bank. Nucleic Acids Res 2000;28(1):235–42.
[25] Mauricio C-T, Shepherd CM, Borelli IA, Venkataraman S, Lander G, Natarajan P, et al. VIPERdb2: an enhanced and web API enabled relational database for structural virology. Nucleic Acids Res 2009;37:D436–42.
[26] Humphrey W, Dalke A, Schulten K. VMD: visual molecular dynamics. J Mol Graph 1996;14(1):33–8.
[27] Phillips JC, Braun R, Wang W, Gumbart J, Tajkhorshid E, Villa E, et al. Scalable molecular dynamics with NAMD. J Comput Chem 2005;26(16):1781–802.
[28] MacKerell AD, Bashford D, Bellott M, Dunbrack RL, Evanseck JD, Field MJ, et al. All-atom empirical potential for molecular modeling and dynamics studies of proteins. J Phys Chem B 1998;102(18):3586–616.
[29] Jorgensen WL, Chandrasekhar J, Madura JD, Impey RW, Klein ML. Comparison of simple potential functions for simulating liquid water. J Chem Phys 1983;79:926 (10 pages).
[30] Feller SE, Zhang Y, Pastor RW, Brooks BR. Constant pressure molecular dynamics simulation: the Langevin piston method. J Chem Phys 1995;103(11):4613–21.

[31] Schlick T, Skeel RD, Brunger AT, Kalé LV, Board JA, Hermans J, et al. Algorithmic challenges in computational molecular biophysics. J Comput Phys 1999;151:9–48.
[32] Altis A, Nguyen PH, Hegger R, Stock G. Dihedral angle principal component analysis of molecular dynamics simulations. J Chem Phys 2007;126:2444111.
[33] Regenmortel MHV. What is a B-cell epitope? Methods Mol Biol 2008:3–20.
[34] Klasse P, Moore J. Quantitative model of antibody- and soluble CD4-mediated neutralization of primary isolates and T-cell line-adapted strains of human immunodeficiency virus type 1. J Virol 1996;70(6):3668–77.
[35] Dimmock NJ. Update on the neutralisation of animal viruses. Rev Med Virol 1995;5(3):165–79.
[36] Han T, Marasco WA. Structural basis of influenza virus neutralization. Ann N Y Acad Sci 2011;1217:178–90.
[37] Burton DR. Antibodies, viruses and vaccines. Nat Rev Immunol 2002;2(9):706–13.
[38] Wang Z, Christensen N, Schiller JT, Dillner J. A monoclonal antibody against intact human papillomavirus type 16 capsids blocks the serological reactivity of most human sera. J Gen Virol 1997;78(9):2209–15.
[39] Culp TD, Spatz CM, Reed CA, Christensen ND. Binding and neutralization efficiencies of monoclonal antibodies, Fab fragments, and scFv specific for L1 epitopes on the capsid of infectious HPV particles. Virology 2007;361(2):435–46.
[40] Sadeyen JR, Tourne S, Shkreli M, Sizaret PY, Coursaget P. Insertion of a foreign sequence on capsid surface loops of human papillomavirus type 16 virus-like particles reduces their capacity to induce neutralizing antibodies and delineates a conformational neutralizing epitope. Virology 2003;309(1):32–40.
[41] Thönes N, Müller M. Oral immunization with different assembly forms of the HPV 16 major capsid protein L1 induces neutralizing antibodies and cytotoxic T-lymphocytes. Virology 2007;369(2):375–88.
[42] Singharoy A, Cheluvaraja S, Ortoleva PJ. Order parameters for macromolecules: application to multiscale simulation. J Chem Phys 2011;134:044104.
[43] Cheluvaraja S, Ortoleva P. Thermal nanostructure: an order parameter/multiscale ensemble approach. J Chem Phys 2010;132(7):075102.